TTMP vol 1(3), 2024
doi: 10.30511/TTMP.2024.2036115,1034

Transactions in Theoretical and Mathematical Physics

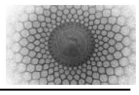

Optical Instabilities in a Media with Quantum Inference Effects in a Micro-Ring Resonator

M.Javad Mohammadpour Nashrudkoli[1,a], M.Reza Poorsadegh bejargafsheh

[1]Department of Physics, University of Guilan, Rasht, Iran

Received: 24 July 2024 / Accepted: 25 August 2024 / Published: 30 August 2024

Abstract We present optical instabilities in a micro-ring resonator filled with media that includes quantum inference effects. The quantum interference effects we consider is a three-level atomic media whose levels are coupled by two laser beams under the Λ-type configuration. Under fast response conditions, we obtain optical instabilities in an all-optical bistable system and study the dynamics of the instability in the regime gain without inversion, which is due to the existence of the Hopf instability in the lower branch of homogeneous stationary state solutions. We also investigated the dynamics of the system under the scan of the control parameter adiabatically, where the temporal oscillations of the intensity are period one, and the phase space of the field is a limit cycle.

1 Introduction

Dynamic behaviour of Optical instability in atom resonator coupled systems has been studied extensively over four decades, particularly in the context of lasers and optical bistability [1–6]. The all-optical bistability (AOB) phenomenon fundamentally affects the cooperative dynamics between atoms and the field. The motivation for the AOB of two-level atoms primarily stems from its prospective applications in all-optical switching, essential for progresses in all-optical communication and computing technologies. Furthermore, AOB elucidates various quantum optical phenomena such as optical instabilities, self oscillations, and chaotic behaviour [7]. Effects of single-mode dynamical instability in a two-level AOB system were first explored in the framework of a plane-wave model. This analysis was subsequently extended to the Gaussian field model addressing its experimental feasibility [8]. Numerous studies have explored the interactions of three-level atomic configuration patterns and multi-mode fields that lead to chaotic behaviour. Savage et al. [9] investigated the possibilities of tri- and quadra-stability alongside the phenomena of self-pulsing and optical turbulence. Similarly, Grangier et al. [10] focused on optical bistability within the dispersive regime and illustrated how chaos can emerge at elevated intensities of the field. Additionally, chaotic behavior has been observed in the Λ configuration pattern of a three-level atomic system where feedback is exclusively applied to the probe field; detuning of the coupling field is employed to induce chaos at higher input intensities [11]. Extensive research has been conducted on cooperative effects and investigating nonlinear dynamical characteristics, including self oscillating and pulsing, instabilities, and chaotic behaviour [12].

The coherent manipulation of quantum states in at-oms and molecules through the coherent light of a laser can give rise to quantum interference in the probability amplitudes of the wave function in transition pathways induced by optical excitation [13]. Quantum interfer-ence and quantum coherence in an atomic system can give rise to numerous significant optical phenomena, such as electromagnetically induced transparency (EIT) [13–16], optical bistability (OB) [17], stimulated Raman adiabatic passage (STIRAP) [18], enhanced index of refraction [19], lasing without inversion [20, 21], etc., were also studied in recent years.

Dynamic of Optical instability, in media that includes quantum inference effects confined in a ring resonator holds substantial theoretical and experimental significance. Investigations on the spatio-temporal dynamics of cavities under such quantum interference effects in 3-level systems began by the Gian-Luca Oppo and were later extended to many important investigations in 2D and 1D [22–26]. These studies considered Λ atomic configuration to realize coherent population trapping and EIT, where many novel phenomena were discovered, yet many other related topics remain to be investigated. However, the nonlinear dynamics of temporal to researchers [27, 28].

[a]e-mail: mj.mohammadpour99@gmail.com

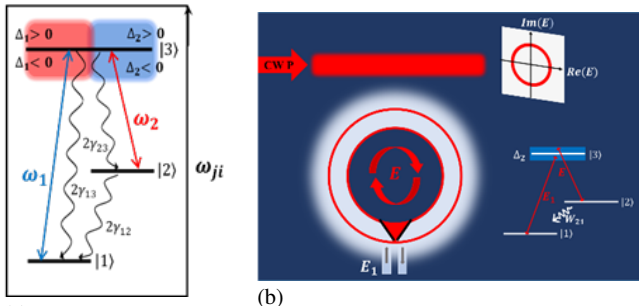

(a) (b)

Figure 1: (a) The Λ coupling pattern of three-level atomic media that interact with the two coherent fields having amplitudes E_1 and E_2 at frequencies ω_1 and ω_2, respectively, and Δ_1 and Δ_2 the respective detuning parameters. (b) A schematic of the micro-ring resonator configuration within pump P and E_1 as input fields, and E as circulating field, filled with media that includes the Λ atomic coupling model with the ground, metastable, and excited states $|1\rangle$, $|2\rangle$, and $|3\rangle$ respectively.

The current study aims to present the instabilities of bistable optical systems in a micro-ring resonator filled with media that includes quantum interference effects. The quantum interference effect we consider is a three-level atomic media whose levels are coupled by two laser beams under the Λ-type coupling pattern. We have identified and explored three regimes of operation depending on the population decay rate of level $|2\rangle$ to level $|1\rangle$ and the ratio of the driving field amplitudes: 1) gain without inversion (this is similar to lasing without inversion), 2) gain with inversion, and 3) inversion without gain. The dynamics of temporal oscillations of the field, which circulates in a resonator, is the focus of our interest. These oscillations arise from the nonlinear reaction of three-level atomic media to the driving fields in the micro-ring resonator in the mean-field limit.

2 Theoretical Model

An alternative promising configuration whose temporal dynamics under the fast response condition in a cavity is not studied is the Λ system, where a single excited upper level (3) is coupled to two lower levels (ground state (1) and meta-stable state (2)). The atomic configuration of interest is shown in Fig. (1.a) and that of the micro-ring resonator containing such medium in Fig. (1.b).

2.1 Interaction Hamiltonian and density matrix

We focus on the Λ coupling pattern of a three level ato-mic system excited by two coherent laser lights with driving frequencies ω_1 and ω_2, as demonstrated in Fig. (1.a). In this study, we employ the semiclassical approach in which the creation and annihilation operators, known as fermion operators, act on an electron at the discrete atomic states. The levels coupled by the driving fields exhibit dipole-allowed transitions; however, the transition from $|1\rangle$ to $|2\rangle$ is dipole-forbidden due to the parity selection rule.

The Hamiltonian that describes the interaction of a three-level atomic configuration, selected from an infinite number of possible levels of an atomic mixed state, with two coherent laser fields treated as classical sources in the rotating-wave approximation, is formulated by appropriately adapting the Hamiltonian of a typical two-level atom-field interaction [29] to the present problem, as follows:

$$\mathscr{H} = \sum_{i=1}^{3} \varepsilon_i a_i^\dagger a_i + \hbar g_1 \left(a_3^\dagger a_1 e^{-i\omega_1 t} + a_1^\dagger a_3 e^{i\omega_1 t} \right) + \hbar g_2 \left(a_3^\dagger a_2 e^{-i\omega_2 t} + a_2^\dagger a_3 e^{i\omega_2 t} \right) \quad (1)$$

Here, ε_i $(i = 1,2,3)$ are the eigenenergies of the discrete atomic states, g_1 and g_2 are the Rabi frequencies of the coupling fields E_1 and E, and $a_i^\dagger = |i\rangle$ and $a_i = \langle i|$ $(i = 1,2,3)$ are electron creation and annihilation operators, respectively.

We note that excitation (de-excitation) of an electron to (from) level $|3\rangle$, corresponding to its creation (removal) in (from) that state, can happen through two routes: $|1\rangle \leftrightarrow |3\rangle$ and $|2\rangle \leftrightarrow |3\rangle$. The full master equation, containing reversible and irreversible parts following the Liouville-von Neumann equation in the interaction picture, can be written as follows:

$$\frac{\partial \rho}{\partial t} = -\frac{i}{\hbar}[\mathscr{H}_I, \rho] + \Lambda\rho, \quad (2)$$

where

$$\mathscr{H}_I = \hbar g_1 \left(a_3^\dagger a_1 e^{-i\Delta_1 t} + a_1^\dagger a_3 e^{i\Delta_1 t} \right) + \hbar g_2 \left(a_3^\dagger a_2 e^{-i\Delta_2 t} + a_2^\dagger a_3 e^{i\Delta_2 t} \right), \quad (3)$$

and the material detunings are defined as $\Delta_1 = \omega_1 - \omega_{31}$ and $\Delta_2 = \omega_2 - \omega_{32}$, with ω_{31} and ω_{32} representing the atomic transition frequencies. Effects of spontaneous emission and complex rate constants are described by Λ_ρ, where the population transition rates between levels i and j are represented by W_{ij} and polarization decay rates by γ_{ij}.

Following the phenomenological approach, and noting that for the three-level case there is more than a single route for a population of a level to change due to spontaneous emission, the density matrix elements, i.e., ρ_{ij} as defined in Eq. (2), contain complex unambiguous time-dependent exponential terms. These can be eliminated using the following transformation:

$$R_{ii} = \rho_{ii} \tag{4a}$$

$$R_{13} = \rho_{13} e^{-i\Delta_1 t} \tag{4b}$$

$$R_{23} = \rho_{23} e^{-i\Delta_2 t} \tag{4c}$$

$$R_{12} = \rho_{12} e^{-i(\Delta_1 - \Delta_2) t} \tag{4d}$$

where R_{ij} denotes the transformed elements of the equation of motion. This simplification significantly improves our capacity to analyze and interpret the behavior of the system. It should be observed that damping rates for coherence terms follow the relation

$$\gamma_{ij} = \frac{1}{2} \sum_k \left(W_{ik} + W_{jk} \right), \tag{5}$$

where the downward population decay rates W_{ij} (with $i > j$) describe the spontaneous decay rate of the excited state. In contrast, excitations from a stable and metastable state to an excited state due to collisional processes have been effectively disregarded, as the energy separations between the levels are significantly greater than kT [30]. Based on this, we arrive at the following expressions:

$$\gamma_{12} = \frac{1}{2} \left(W_{12} + W_{13} + W_{21} + W_{23} \right) \approx \frac{W_{21}}{2}, \tag{6}$$

$$\gamma_{13} = \frac{1}{2} \left(W_{12} + W_{13} + W_{31} + W_{32} \right) \approx \frac{W_{31} + W_{32}}{2}, \tag{7}$$

$$\begin{aligned} \gamma_{23} &= \frac{1}{2} \left(W_{21} + W_{23} + W_{31} + W_{32} \right) \\ &\approx \frac{W_{21} + W_{31} + W_{32}}{2}, \end{aligned} \tag{8}$$

$$\Psi = \left(\alpha_{12} \cdot \beta_{12} \cdot \alpha_{13} \cdot \beta_{13} \cdot \alpha_{23} \cdot \beta_{23} \cdot R_{22} \cdot R_{33} \right)^T, \tag{9}$$

Eq. (2) leads to 8 linear time-independent equations for the transformed elements of the equation of motion R_{ij} in the form of $\partial_t \Psi = M\Psi + I$. At steady state, we have:

$$(-2g_2)\beta_{23} - W_{21}R_{22} + W_{32}R_{33} = 0, \tag{10.a}$$

$$(2g_1)\beta_{13} + (2g_2)\beta_{23} - (W_{31} + W_{32})R_{33} = 0, \tag{10.b}$$

$$(\Delta_1 - \Delta_2)\alpha_{12} + \gamma_{12}\beta_{12} - g_2\alpha_{13} + g_1\alpha_{23} = 0, \tag{10.c}$$

$$\gamma_{12}\alpha_{12} + (\Delta_2 - \Delta_1)\beta_{12} + g_2\beta_{13} + g_1\beta_{23} = 0, \tag{10.d}$$

$$g_2\beta_{12} + \gamma_{13}\alpha_{13} - \Delta_1\beta_{13} = 0, \tag{10.e}$$

$$-g_2\alpha_{12} + \Delta_1\alpha_{13} + \gamma_{13}\beta_{13} + g_1R_{22} + 2g_1R_{33} = g_1, \tag{10.f}$$

$$g_1\beta_{12} - \gamma_{23}\alpha_{23} + \Delta_2\beta_{23} = 0, \tag{10.g}$$

$$g_1\alpha_{12} - \Delta_2\alpha_{23} - \gamma_{23}\beta_{23} + g_2R_{22} - g_2R_{33} = 0, \tag{10.h}$$

where α_{ij} and β_{ij} are the real and imaginary parts of R_{ij}. Steady-state solutions can be obtained by considering $R_{11} = 1 - R_{22} - R_{33}$, $R_{ij} = R_{ji}^*$, $W_{31} = 1$, and $\Delta_1 = 0$, in the form of $M\Psi = -I$, through the coefficient matrix method, where:

$$M = \begin{bmatrix} 0 & 0 & 0 & 0 & 0 & -2g_2 & -W_{21} & W_{32} \\ 0 & 0 & 0 & 2g_1 & 0 & 2g_2 & 0 & -(W_{32}+1) \\ -\Delta_2 & \gamma_{12} & -g_2 & 0 & g_1 & 0 & 0 & 0 \\ \gamma_{12} & \Delta_2 & 0 & g_2 & 0 & g_1 & 0 & 0 \\ 0 & g_2 & \gamma_{13} & 0 & 0 & 0 & 0 & 0 \\ -g_2 & 0 & 0 & \gamma_{13} & 0 & 0 & g_1 & 2g_1 \\ 0 & g_1 & 0 & 0 & -\gamma_{23} & \Delta_2 & 0 & 0 \\ g_1 & 0 & 0 & 0 & -\Delta_2 & -\gamma_{23} & g_2 & -g_2 \end{bmatrix} \tag{11}$$

and

$$I = \begin{pmatrix} 0 & 0 & 0 & 0 & 0 & g_1 & 0 & 0 \end{pmatrix}^T, \tag{12}$$

where the dispersion (α_{ij}) and absorption (β_{ij}) coefficients are given in the Appendix. Note that all the parameters in our calculations have been normalized to γ.

2.2 Main Model

The schematic of the micro-ring resonator, in which media that includes quantum interference effects is confined, is displayed in Fig. (1.b). The resonator has two inputs: one at the top from a straight waveguide and the other at the bottom of the ring. The quantum interference effects we consider involve a three-level atomic medium whose levels are coupled by two laser beams under the Λ-type coupling pattern, as illustrated schematically in Fig. (1.a) with decay mechanisms. States $|1\rangle$ and $|2\rangle$ are the ground and metastable states, respectively, while state $|3\rangle$ is an excited state. The transitions $|1\rangle \rightarrow |3\rangle$ and $|2\rangle \rightarrow |3\rangle$ have opposite parity, while $|1\rangle \rightarrow |2\rangle$ has the same parity.

The maser field E circulates within the ring resonator, externally pumped by a continuous wave (CW) source proportional to P, and couples the metastable state $|2\rangle$ and the excited state $|3\rangle$. The pump field is coupled to the resonator from the top of the ring in Fig. (1.b), and after light-matter interaction, it propagates as field E. The micro-ring resonator, schematically shown in Fig. (1.b), is designed to keep the field E inside the resonator, repeating the light-matter interaction after each round trip of a photon along the ring. Meanwhile, the field E_1, after coupling the ground and excited states under a technique, is directed out of the resonator and does not circulate along the ring. This technique is effective when the field E_1 is prepared with polarization opposite to that of field E.

Identifying the field that should circulate within the ring and the field that must exit without circulating relies on the beam splitter embedded within the micro-ring resonator, indicated by the black lines at the ring's bottom in Fig. (1.b). Due to the significant frequency difference between E and E_1 [refer to Fig. (1.a)], they do not significantly influence each other, allowing any minor effects to be disregarded.

In the case where the response of the atomic medium is faster than the micro-resonator lifetime (fast-response condition) and in the anomalous dispersion regime, the dynamics of the beam propagating in such a resonator are described in the mean-field limit with the Lugiato-Lefever equation (LLE) [31]:

$$\partial_t E = P - (1 + i\theta)E + (2C)iR_{23} + i\nabla^2 E, \tag{13}$$

where ∂_t represents the slow time over multiple round trips within the resonator. P denotes the amplitude of the input pump and is a fraction of field E, and θ indicates the detuning between the cavity resonant frequency and input frequency, which we use as the control parameter in our simulations. The transverse diffraction of the master field in two dimensions is described using the Laplacian. Finally, $2C$ describes the cooperativity parameter of the light-matter interaction, given by

$$2C = \frac{N\mu^2 kL}{2\hbar\gamma\varepsilon_0 T}, \tag{14}$$

where μ represents the transition dipole moment, k denotes the field wave number, L is the resonator length, γ describes the atomic linewidth, ε_0 indicates the permittivity of free space, and T is the resonator transmissivity. Every physical parameter in Eq. (13) has been scaled through appropriate normalizations, per standard methods for operating the mean-field or LLE model [31].

Details of the spatio-temporal dynamics of such a model are provided in Refs. [23, 25]. In this work, we ignore any spatial dependence of the field within the resonator; in fact, we consider the classical field circulating inside the ring resonator to be homogeneous and ignore the transverse diffraction of the field, setting the diffraction operator in Eq. (13) to $\nabla^2 = 0$. This reduction simplifies the system's dynamics from spatio-temporal to temporal, allowing us to investigate the evolution of temporal oscillations and optical instabilities as the detuning θ is varied as a control parameter.

We focus on the evolution of the driving field coupling states $|3\rangle \rightarrow |2\rangle$ [see Fig. (1.a)]. We also consider a fast medium where the atomic variables (level populations and coherences) quickly relax to their stationary values. This allows light propagating through the medium to experience absorption (gain) and refraction characterized by the density matrix element R_{23}. We utilize the expression for R_{23} (see Appendix) for the nonlinear response in the ring resonator, where the dynamics of the field E are described by the mean-field equation.

As mentioned above, our goal is to study optical instabilities in an all-optical bistable system. To do this, we first need to find homogeneous stationary solutions (HSS) derived from Eq. (13) by setting $\partial_t = 0$ and $\nabla^2 = 0$:

$$|P|^2 = \left[(1 + 2C\mathrm{Im}(\chi))^2 + (\theta - 2C\mathrm{Re}(\chi))^2\right]|E_s|^2, \tag{15}$$

where $\mathrm{Re}(\chi)$ and $\mathrm{Im}(\chi)$ are the real and imaginary parts of the electric susceptibility in R_{12} (see Appendix). We also set $2C = 30$ and use the resonator detuning θ as the control parameter of the atom-field-resonator system, as is commonly done in experiments. The values of Δ_2, W_{32}, W_{21}, P, and E_1 will be chosen based on the regime of interest later.

In our simulations, we employed the second order Runge Kutta algorithm to integrate Eq. (13) self consistently without the diffraction operator. We must highlight that we incorporated the coherence term (off-diagonal density matrix element) into the mean field using steady-state solutions (see Appendix).

3 Results and Discussion

As shown schematically in Fig. (1.a), we are interested in the evolution of the driving field coupling states $|2\rangle \rightarrow |3\rangle$ (denoted as E) with the Rabi frequency g_2. One of the fascinating predictions from [30] regarding Λ and Ξ atomic configurations is the amplification of a weak probe field across a broad frequency ranges of the absorption feature. In this study, the three-level atoms play the role of active medium. This occurs when the dressed atomic states are driven towards an inverted state, which necessitates fulfilling the condition [30].

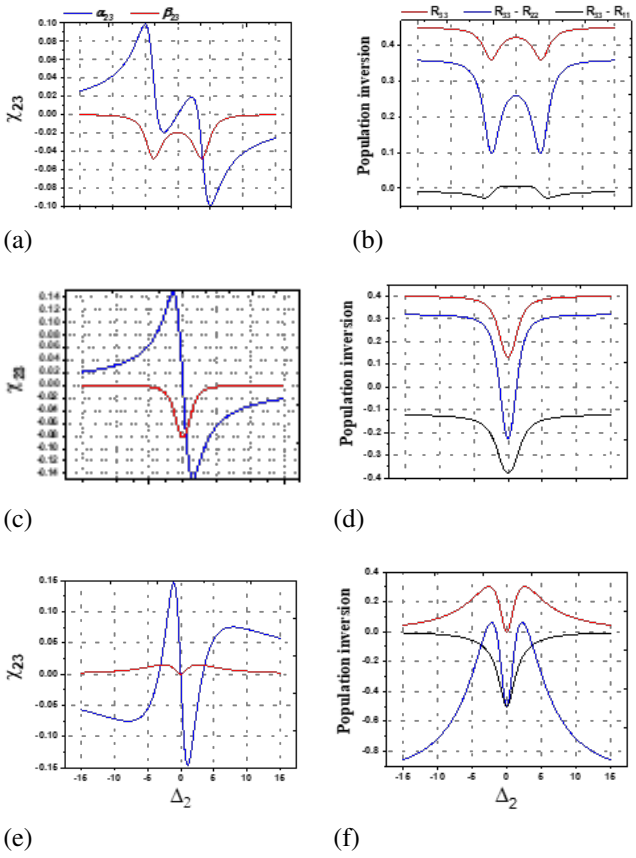

Figure 2: The electric susceptibility and Population inversion in the two allowed transitions and population of the exited state versus the material detuning. (a, b) gain in the presence of inversion $W_{21} = 0.5$, $W_{32} = 0.1$, $E_1 = 4$, $E = 1$, (c, d) gain in absence of inversion with $W_{21} = 0.5$, $W_{32} = 0.1$, $E_1 = E = 1$ and (e, f) inversion without gain $W_{21} = 0$, $W_{32} = 0.1$, $E_1 = E = 1$.

The findings from [30] regarding Λ and Ξ atomic configurations highlight the amplification of a weak probe field across a broad frequency range of the absorption feature. In this study, the three-level atoms function as the active medium. This amplification occurs when the dressed atomic states are driven towards an inverted state, which necessitates fulfilling the condition [30]:

$$\frac{W_{21} - W_{32}}{1 + W_{21}} > \left(\frac{E}{E_1}\right)^2, \tag{12}$$

This phenomenon significantly differs from what is typically observed in two-level systems. Firstly, two-level atoms generate gain rather than absorption in response to a probe, but only within specific frequency ranges. Secondly, it involves a parametric energy transfer from the pump to the probe, mediated by atomic susceptibility. On the other hand, for the three-level system, the gain arises from an inversion state between the levels of the excited atoms.

Based on condition (12), as shown in Fig. 2, we have identified and explored three regimes of operation depending on the population decay rate of level $|2\rangle$ to level $|1\rangle$ and the ratio of the driving field amplitudes:

i) Gain with population inversion in the $|2\rangle \rightarrow |3\rangle$ transition,
ii) Gain without population inversion (this is similar to lasing without inversion),
iii) Population inversion without gain.

Fig. 2 shows the steady-state solutions for absorption, dispersion profile, and population inversion along Δ_2. If we follow condition (12), then gain ($\beta_{23} < 0$) is achievable in the presence of population inversion ($R_{33} - R_{22} > 0$ & $R_{33} - R_{11} > 0$) [refer to Figs (2.a) and (2.b)]. However, if we relax the strict condition of Eq. (12) when choosing the strength of the driving fields, we arrive at a situation where population inversion ($R_{33} - R_{22} < 0$ & $R_{33} - R_{11} < 0$) is reversed around the resonance while gain ($\beta_{23} < 0$) is still established. In Figs (2.c) and (2.d), we have chosen equal values for the driving fields $E_2 = E_1 = 1$ while keeping the other parameters the same as in Figs (2.a) and (2.b). It is observed that around the resonance of the $|2\rangle \rightarrow |3\rangle$ transition, population inversion is absent but is obtained everywhere when Δ_2 moves far from resonance. The next regime, shown in Figs (2.e) and (2.f), is realized when no population decay is allowed from level $|2\rangle$ to level $|1\rangle$ (i.e., $W_{21} = 0$). In this case, gain is removed everywhere while population inversion can still be obtained far from the resonance of the $|3\rangle \rightarrow |2\rangle$ transition, a phenomenon that has been extensively studied. This also represents the "Raman transition," the result of which is coherent population trapping, and is realized when the population decay rate of level $|2\rangle$ to level $|1\rangle$ is considered zero ($W_{21} = 0$). In Fig. 3, the homogeneous stationary states (HSS) evolve with cavity detuning θ at the maximum gain, i.e., $\Delta_2 = 0.467$, according to Eq. (15), where a clear bistability is seen for negative cavity detuning values. In this study, our results are based on the values of

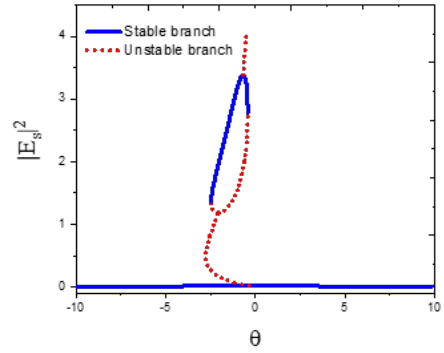

Figure 3: Bistability of the HSS in terms of cavity detuning. Parameter values are similar to Figs (2.c) and (2.d) with $\Delta_2 = 0.467$.

the parameters in the regime of gain without inversion, similar to lasing without inversion. As mentioned, we keep Δ_2 in the region where no inversion is expected while the gain is close to its maximum value. A wide bistability is obtained for the HSS solutions. The stable and unstable branches of The solutions are clearly defined. At $\theta = -2.462$, the system switches from the lower branch to the upper branch, and at $\theta = -0.425$ from the upper branch to the lower branch of the bistable diagram, or vice versa, so the bistable threshold is in the form of $-2.462 < \theta < -0.425$.

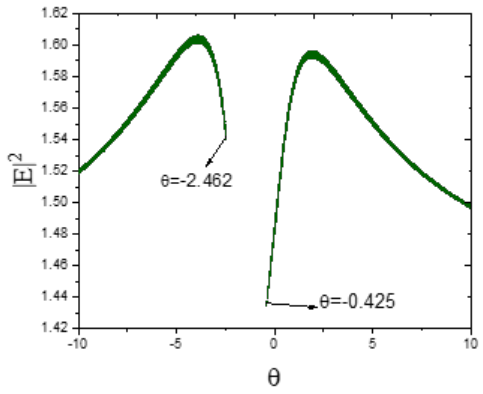

Figure 4: Field intensity, under the adiabatic scan of the resonator detuning. The parameter values in this figure are similar to those in Fig. 3.

In Fig. 4, we simulated the time-dependent field E based on Eq. (14) and kept the parameter values similar to Figs (3.c) and (3.d); we started the simulation from noise under the adiabatic scan $-10 < \theta < 10$. The simulation result and the homogeneous stationary solutions coincide and show a clear range for the bistable threshold and self-pulsing solutions.

During the scan of the control parameter, only a period-one path for the field intensity appears, which is representative of the limit cycle. This oscillation disappears at the bistable threshold, which is due to the absence of Hopf instability in the upper branch of the HSS solutions.

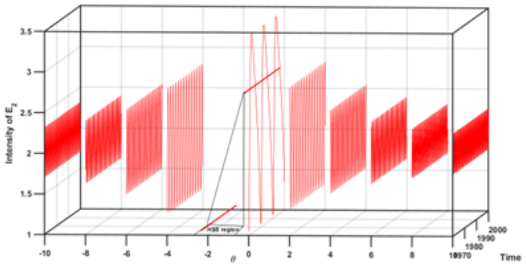

(a)

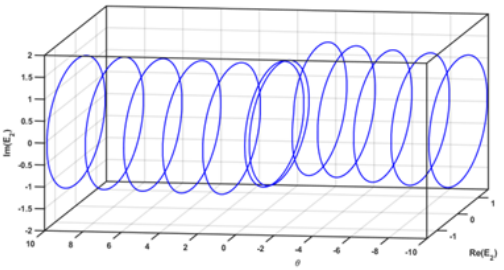

(b)

Figure 5: (a) Time trace, and (b) The limit cycle continuation from the Hopf (H) point at the very onset of instability on the lower branch of the OB curve shown in Fig. 3. Parameter values are similar to Fig. 3.

Figs (5.a) and (5.b) show the intensity-time and phase space of the field, respectively. From Fig. (5.a), it is concluded that from negative and positive values of θ, the oscillation frequency decreases and increases, respectively, at the bistable threshold due to moving away from the Hopf instability point in the lower branch. Fig. (5.b) shows the phase space of the complex field, which illustrates the limit cycles in the range of $-10 < \theta < 10$, where the radius of the cycles increases as the bistable threshold is approached, indicating an increase in the amplitude of oscillations in this range.

Bistability for input (P) and output (E_s) field intensities is shown in Fig. 6. Under a certain value of the input field, by increasing or decreasing θ as a control parameter, the output field increases and decreases respectively. The boundary of these changes is the bistable threshold of Fig. 3, which is the same interpretation for the other side. Thus, by reducing or increasing θ, the output intensity value can be controlled under the input intensity.

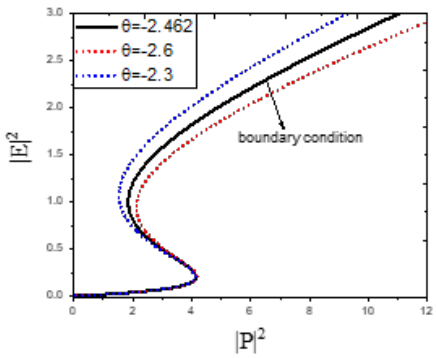

Figure 6: Bistability in the input and output intensities with $\theta = -2.462$ as a boundary condition. Other parameter values in this figure are similar to those in Fig. 3.

4 Conclusions

Our results indicate that the intensity of the output field from the micro-ring resonator, influenced by quantum interference effects, exhibits oscillations if the fields used to couple the atomic levels are considered continuous waves (CW). This behavior arises from the Hopf instability in the lower branch of the bistable dia-gram, attributed to the gain present in this regime. We identified a single type of periodic solution (one-periodic with a limit cycle) in the system dynamics, as we considered a fast medium where the atomic varia-bles (level populations and coherences) quickly relax to their stationary values, facilitating the propagation of light through the medium. Notably, we demonstrated a system with self-oscillating dynamics by exploring the gain regime without population inversion, which allows for utilization in all-optical communication and cir-cuits. Furthermore, we provide evidence that the output intensity of the resonator can be controlled by adjusting the resonator detuning.

Acknowledgements We gratefully acknowledge Dr. Mansour Eslami for his valuable guidance and insights.

Appendix

It should be mentioned that off-diagonal variables being complex are written in the following form:

$$R_{23} = \alpha_{23} + i\beta_{23}, \tag{A1}$$

$$R_{13} = \alpha_{13} + i\beta_{13}, \tag{A2}$$

$$R_{12} = \alpha_{12} + i\beta_{12}, \tag{A3}$$

which are proportional to the field amplitude E_1 and E via [29]:

$$R_{23} = \chi_{23}E, \tag{A4}$$

$$R_{12} = \chi_{13}E_1, \tag{A5}$$

In this section, we solve the coefficients matrix (Eq. (10)) using MATLAB software and obtain the absorption and dispersion coefficients for the transition between the levels, as well as the population equations for all three levels, and in a simplified form, we have:

$$\begin{aligned}
D = {} & 2g_2g_1^6\gamma_{13}(2W_{21}+W_{32}) + g_2(W_{21}\gamma_{13}^2 + 2g_2^2\gamma_{13} + W_{21}W_{32}\gamma_{13}^2 - 8W_{21}\Delta_2^2\gamma_{13} - 4W_{32}\Delta_2^2\gamma_{13})g_1^4 \\
& + g_2(-6W_{21}g_2^2\gamma_{13} + 4W_{21}g_2^2\gamma_{23} + 2W_{32}g_2^2\gamma_{13} + 2W_{32}g_2^2\gamma_{23} + 12g_2^2\gamma_{12}\gamma_{13})g_1^4 + g_2(8W_{21}\gamma_{12}\gamma_{13}\gamma_{23} + 4W_{32}\gamma_{12}\gamma_{13}\gamma_{23} \\
& + 2g_2^4\gamma_{13} + 2g_2^4\gamma_{23} - 2W_{21}\Delta_2^2\gamma_{13}^2)g_1^2 + g_2(-2\Delta_2^2g_2^2\gamma_{13} + 2g_2^2\gamma_{12}\gamma_{13}^2 + 4W_{21}\Delta_2^4\gamma_{13} + 2W_{32}\Delta_2^4\gamma_{13} \\
& + 2W_{21}g_2^4\gamma_{13})g_1^2 + g_2(-6W_{21}g_2^4\gamma_{23} + 2W_{32}g_2^4\gamma_{23} + 12g_2^4\gamma_{12}\gamma_{23} + 2W_{21}g_2^2\gamma_{13}\gamma_{23} + 2W_{21}\gamma_{12}\gamma_{13}^2\gamma_{23})g_1^2 \\
& + g_2(2g_2^2\gamma_{12}\gamma_{13}\gamma_{23} - 2W_{21}W_{32}\Delta_2^2\gamma_{13}^2 + 4W_{21}\Delta_2^2g_2^2\gamma_{12} + 6W_{21}\Delta_2^2g_2^2\gamma_{13} + 2W_{32}\Delta_2^2g_2^2\gamma_{12})g_1^2 \\
& + g_2(-2W_{32}\Delta_2^2g_2^2\gamma_{13} + 4W_{21}\Delta_2^2\gamma_{12}^2\gamma_{13} + 4W_{21}\Delta_2^2\gamma_{13}\gamma_{23}^2 + 2W_{32}\Delta_2^2\gamma_{12}^2\gamma_{13} + 2W_{32}\Delta_2^2\gamma_{13}\gamma_{23}^2)g_1^2 \\
& + g_2(2W_{21}g_2^2\gamma_{12}\gamma_{13}^2 + 4W_{21}g_2^2\gamma_{12}\gamma_{23}^2 + 2W_{32}g_2^2\gamma_{12}\gamma_{23}^2 + 4W_{21}\gamma_{12}^2\gamma_{13}\gamma_{23}^2 + 2W_{32}\gamma_{12}^2\gamma_{13}\gamma_{23}^2)g_1^2 \\
& + g_2(12\Delta_2^2g_2^2\gamma_{13}\gamma_{23} + 12g_2^2\gamma_{12}^2\gamma_{13}\gamma_{23} + 2W_{21}W_{32}g_2^2\gamma_{13}\gamma_{23} + 2W_{21}W_{32}\gamma_{12}\gamma_{13}^2\gamma_{23}^3 - 6W_{21}g_2^2\gamma_{12}\gamma_{13}\gamma_{23})g_1^2 \\
& + g_2(2W_{32}g_2^2\gamma_{12}\gamma_{13}\gamma_{23} + 2g_2^6\gamma_{23} + W_{21}\Delta_2^2g_2^4 + W_{21}\Delta_2^4\gamma_{13}^2 + W_{21}g_2^4\gamma_{23}^2) + g_2(2W_{21}g_2^6\gamma_{23} + W_{21}\Delta_2^2\gamma_{12}^2\gamma_{13}^2 \\
& + W_{21}\Delta_2^2\gamma_{13}^2\gamma_{23}^2 + W_{21}\gamma_{12}^2\gamma_{13}^2\gamma_{23}^2 + 2\Delta_2^2g_2^2\gamma_{13}^2\gamma_{23}) + g_2(2g_2^2\gamma_{12}^2\gamma_{13}\gamma_{23} + 4g_2^4\gamma_{12}\gamma_{13}\gamma_{23} + W_{21}W_{32}\Delta_2^2g_2^4 \\
& + W_{21}W_{32}\Delta_2^4\gamma_{13}^2 + W_{21}W_{32}g_2^4\gamma_{23}^2) + g_2(2W_{21}\Delta_2^2g_2^2\gamma_{12}\gamma_{13} + 2W_{21}g_2^2\gamma_{12}\gamma_{13}\gamma_{23}^2 + W_{21}W_{32}\Delta_2^2\gamma_{12}^2\gamma_{13}^2 + W_{21}W_{32}\Delta_2^2\gamma_{13}^2\gamma_{23}^2 \\
& + W_{21}W_{32}\gamma_{12}^2\gamma_{13}^2\gamma_{23}^2) + g_2(2W_{21}\Delta_2^2g_2^2\gamma_{13}^2\gamma_{23} + 2W_{21}\gamma_{12}^2\gamma_{13}^2\gamma_{23} + 4W_{21}g_2^4\gamma_{12}\gamma_{13}\gamma_{23}) + 2W_{21}W_{32}\Delta_2^2g_2^2\gamma_{12}\gamma_{13} \\
& + 2W_{21}W_{32}g_2^2\gamma_{12}\gamma_{13}\gamma_{23}^2
\end{aligned} \tag{A6}$$

$$\begin{aligned}\tilde{\alpha}_{23} = \Delta_2 g_2 \{ & g_1^4 \gamma_{13}(W_{21} - W_{32}) + 2(W_{32} - W_{21}) \\ & \times \left(g_2^2 \gamma_{12} + \Delta_2^2 \gamma_{13}\right) + 2(W_{32} - W_{21}) \gamma_{12}^2 \times \gamma_{13} \\ & - g_2 \left[(1 + W_{21}) \times \gamma_{13} - (W_{32} + 1) \times W_{21}\right] \\ & - W_{21} \times \gamma_{12}(\gamma_{13} + \gamma_{23}) \\ & - W_{21} W_{32} \times \gamma_{13}(\gamma_{12} + \gamma_{23}) g_1^2 \}\end{aligned} \tag{A7}$$

$$\begin{aligned}\tilde{\beta}_{23} = & g_1^4 g_2 \gamma_{13} \left[2\gamma_{12}(W_{32} - W_{21}) - W_{21}(W_{32} + 1)\right] \\ & + \left[g_2 W_{21}(\Delta_2^2 \gamma_{13} - g_2^2 \gamma_{23})(W_{32} + 1)\right. \\ & + 2 g_2 \gamma_{23}(W_{32} - W_{21})(g_2^2 \gamma_{12} + \Delta_2^2 \gamma_{13} + \gamma_{12}^2 \gamma_{13}) \\ & \left. - (W_{32} + W_{21}) g_2 \gamma_{12} \gamma_{13} \gamma_{23}\right] g_1^2,\end{aligned} \tag{A8}$$

$$\begin{aligned}\tilde{\alpha}_{13} = & g_1^3 g_2^2 \left[2W_{32}\Delta_2(\gamma_{12} + \gamma_{23}) - W_{21}\Delta_2 \times \right. \\ & \left. (W_{32} + 2\gamma_{12} + 2\gamma_{23} + 1)\right] + g_1 g_2^2 \Delta_2 \times \\ & \left[W_{21}\left(\Delta_2^2(1 + W_{32}) + \gamma_{23}^2(1 + W_{32})\right)\right. \\ & \left. + 2 g_2^2 \gamma_{23}(1 + W_{21})\right],\end{aligned} \tag{A9}$$

$$\begin{aligned}\tilde{\beta}_{13} = & g_1^5 (W_{21}\gamma_{13})(1 + W_{32}) + g_1^3 \left[W_{21}(1 + W_{32})\right. \\ & \times \left(g_2 \gamma_{23} + 2\gamma_{13}(\gamma_{12}\gamma_{23} - \Delta_2^2)\right) \\ & \left. + 2 g_2^2 \gamma_{12} \gamma_{13}(1 + W_{21})\right] \\ & + g_1 \left[(1 + W_{21})\left(2 g_2^4 \gamma_{12}\gamma_{23} + 4 g_2^2 \gamma_{13}\gamma_{23}\right)\right. \\ & \times \left(\Delta_2^2 + \gamma_{12}^2\right) \\ & + W_{21}\gamma_{13}(1 + W_{32})\left(\Delta_2^4 + (\gamma_{12}\gamma_{23})^2\right) \\ & \left. + g_2^2 W_{21}\gamma_{12}(\Delta_2^2 + \gamma_{23}^2)\right] \\ & + W_{21}\Delta_2^2 \gamma_{13}(\gamma_{12}^2 + \gamma_{23}^2),\end{aligned} \tag{A10}$$

$$\begin{aligned}\tilde{\alpha}_{12} = g_1 g_2 \{ & (W_{21} - W_{32}) \times (2\gamma_{13} g_1^4 + 2 g_1^2 g_2^2 \gamma_{23}) \\ & + \gamma_{13} g_1^2 \times (2\gamma_{12}\gamma_{23} - 2\Delta_2^2) \\ & - (W_{21} + 1) \times (2 g_1^2 g_2^2 \gamma_{13} + 2 g_2^4 \gamma_{23}) \\ & + g_2^2 \times (\gamma_{12}\gamma_{13}\gamma_{23}) - (1 + W_{32}) \\ & \times (\gamma_{13} g_1^2 W_{21}\gamma_{23} - g_2^2 W_{21}\Delta_2^2) \\ & - W_{21}\gamma_{12}\gamma_{13} \times (\gamma_{23}^2 + \Delta_2^2)\} + W_{21} + \gamma_{23}^2,\end{aligned} \tag{A11}$$

$$\begin{aligned}\tilde{\beta}_{12} = & g_1^3 g_2 \Delta_2 \gamma_{13} \left[W_{21} \times (1 + W_{32} + 2(\gamma_{12} + \gamma_{23}))\right. \\ & \left. - 2W_{32} \times (\gamma_{12} + \gamma_{23})\right] \\ & - g_1 g_2 \times (1 + W_{32}) W_{21}\Delta_2\gamma_{13} \times (\Delta_2 + \gamma_{23}^2) \\ & + 2 g_1 g_2 \times (1 + W_{21})(\Delta_2 \gamma_{13}\gamma_{23}),\end{aligned} \tag{A12}$$

$$\begin{aligned}\tilde{R}_{22} = & 2 g_1^6 W_{32}\gamma_{13} + g_2 g_1^4 \left(2 g_2^2 \gamma_{13} \times (1 + 2\gamma_{12})\right. \\ & \left. + 2W_{32} \times \left(g_2^2 \gamma_{23} + 2\gamma_{12}\gamma_{13}\gamma_{23} - 2\Delta_2^2 \gamma_{13}\right)\right) \\ & + g_2 g_1^2 \left[2W_{32} \times \left(\gamma_{13}\Delta_2^2(\Delta_2^2 + \gamma_{23}^2)\right)\right. \\ & + g_2^2 \gamma_{12}(\Delta_2^2 + \gamma_{23}^2) + \gamma_{13}\gamma_{12}^2(\Delta_2^2 + \gamma_{23}^2)\left.\right] \\ & + 4\gamma_{13}\Delta_2^2 g_2^2 \gamma_{23} + (1 + 2\gamma_{12}) \times 2 g_2^4 \gamma_{23} \\ & \left. + 2 g_2^2 \gamma_{13} \times \left(\gamma_{12}\gamma_{23} + 2\gamma_{12}^2 \gamma_{23} - \Delta_2^2\right)\right],\end{aligned} \tag{A13}$$

$$\begin{aligned}\tilde{R}_{33} = & 2W_{21} g_1^6 g_2 \gamma_{13} + g_1^4 g_2 \left(2W_{21} g_2^2 (\gamma_{23} - \gamma_{13})\right. \\ & \left. + 4\gamma_{13} \times (W_{21}(\gamma_{12}\gamma_{23} - \Delta_2^2) + g_2^2 \gamma_{12})\right) \\ & + g_2 \left[2W_{21} \times \left(\gamma_{13}\Delta_2^4 + \Delta_2^2 g_2^2 \gamma_{12} + g_2^2 \gamma_{12}\gamma_{23}^2\right.\right. \\ & + \gamma_{13}\gamma_{12}^2 \gamma_{23^2} + \gamma_{13}\Delta_2^2 \gamma_{23}^2 - \gamma_{13} g_2^2 \gamma_{12}\gamma_{23}\left.\right) \\ & \left. + \gamma_{13}\Delta_2^2(g_2^2 + \gamma_{12}^2)\right] + 4 g_2^2 \gamma_{13}\gamma_{23} \\ & \left. \times (\Delta_2^2 + \gamma_{12}^2) + 2 g_2^4 \gamma_{23} \times (2\gamma_{12} - W_{21})\right] g_1^2.\end{aligned} \tag{A14}$$

$$R_{ii} = \frac{\tilde{R}_{ii}}{D}, \tag{A15}$$

$$\alpha_{ij} = \frac{\tilde{\alpha}_{ij}}{D}, \tag{A16}$$

$$\beta_{ij} = \frac{\tilde{\beta}_{ij}}{D}, \tag{A17}$$

References

1. F. T. Arecchi and R. G. Harrison, *Instabilities and Chaos in Quantum Optics*, Springer Science, 2012.
2. H. Haken, Zeitschrift für Physik, **190**, 3, (1966)
3. A. Joshi and M. Xiao, J. Modern Opt. **57**, 14, (2010)
4. G. Khitrova, J. Valley, and H. Gibbs, Phys. Rev. Lett. **60**, 12 (1988)
5. L. A. Lugiato et al., Opt. Commun. **43**, 4, (1982)
6. G. H. Van Tartwijk and G. P. Agrawal, Prog. in Quant. Elec. **22**, 2 (1998)
7. K. Osman and Joshi, Phys. Lett. A, **376**, 37 (2012)
8. L. Orozco et al., Phys. Rev. A, **39**, 3 (1989)
9. C. Savage, H. Carmichael, and D. Walls, Opt. Comm., **42**, 3 (1982)
10. P. Grangier, J. Roch, J. Roger, L. Lugiato, E.M. Pessina, G. Scandroglio, and P. Galatola, Phys. Rev. A, **46**, (1992)
11. W. Yang, Joshi, and M. Xiao, Phys. Rev. Lett., **95**, 9 (2005)
12. H. M. Gibbs et al., Phys. Rev. Lett., **46**, 7 (1981)

13. M. Fleischhauer, Imamoglu, and J. P. Marangos, Rev. Mod. Phys., **77**, 2 (2005)
14. K. J. Boller, Imamoğlu, and S.E. Harris, Phys. Rev. Lett., **66**, 20 (1991)
15. S. E. Harris, Phys. Today, **50**, 7 (1997)
16. Kasapi et al., Phys. Rev. Lett., **74**, 13 (1995)
17. Rosenberger, L. Orozco, and H. Kimble, Phys. Rev. A, **28**, 4 (1983)
18. N. V. Vitanov et al., Rev. Mod. Phys., **89**, 1 (2017)
19. M. O. Scully, Phys. Rev. Lett., **67**, 14 (1991)
20. J. Mompart, C. Peters, and R. Corbalán, Phys. Rev. A, **57**, 3 (1998)
21. Vladimirov et al., Phys. Rev. E, **57**, 2 (1998)
22. M. Eslami et al., Phys. Rev. A, **108**, 5 (2023)
23. M. Eslami et al., Phys. Rev. A, **90**, 2 (2014)
24. M. Eslami, R. Kheradmand, and G. Oppo, J. Phys. B: At. Mol. Opt. Phys., **53**, 7 (2020)
25. G. L. Oppo, J. Mod. Opt., **57**, 14-15 (2010)
26. G. L. Oppo, D. Grant, and M. Eslami, Phys. Rev. A, **105**, 1 (2022)
27. H. Babu and H. Wanare, Phys. Rev. A, **88**, 2 (2013)
28. H. Babu and H. Wanare, Phys. Rev. A, **83**, 3 (2011)
29. M. O. Scully and M. S. Zubairy, *Quantum optics* (Cambridge University Press, 1997).
30. Manka et al., Phys. Rev. A, **43**, 7 (1991)
31. M. Haelterman, S. Trillo, and S. Wabnitz, Opt. Comm., **91**, 5-6 (1992)